Optimal control of quantum-mechanical systems: Existence, numerical approximation, and applications

Anthony P. Peirce and Mohammed A. Dahleh
Program in Applied and Computational Mathematics, Princeton University, Princeton, New Jersey 08544

Herschel Rabitz
Department of Chemistry, Princeton University, Princeton, New Jersey 08544
(Received 21 October 1987)

The optimal control of the path to a specified final state of a quantum-mechanical system is investigated. The problem is formulated as a minimization problem over appropriate function spaces, and the well-posedness of this problem is is established by proving the existence of an optimal solution. A Lagrange-multiplier technique is used to reduce the problem to an equivalent optimization problem and to derive necessary conditions for a minimum. These necessary conditions form the basis for a gradient iterative procedure to search for a minimum. A numerical scheme based on finite differences is used to reduce the infinite-dimensional minimization problem to an approximate finite-dimensional problem. Numerical examples are provided for final-state control of a diatomic molecule represented by a Morse potential. Within the context of this optimal control formulation, numerical results are given for the optimal pulsing strategy to demonstrate the feasibility of wave-packet control and finally to achieve a specified dissociative wave packet at a given time. The optimal external optical fields generally have a high degree of structure, including an early time period of wave-packet phase adjustment followed by a period of extensive energy deposition to achieve the imposed objective. Constraints on the form of the molecular dipole (e.g., a linear dipole) are shown to limit the accessibility (i.e., controllability) of certain types of molecular wave-packet objectives. The nontrivial structure of the optimal pulse strategies emphasizes the ultimate usefulness of an optimal-control approach to the steering of quantum systems to desired objectives.

I. INTRODUCTION

The search for the appropriate excitation of molecular-scale physical systems to achieve certain objectives has recently been the subject of increased interest. Examples include the design of pulse strategies for nuclear-magnetic-resonant (NMR) imaging sequences[1-3] and the use of lasers to achieve site-specific excitations or dissociation in polyatomic molecules.[4]

The approach often adopted has been to use physical intuition in the design of appropriate excitation strategies. Results to date based on physically motivated guesses for optical pumping strategies have been disappointing. If such problems have a solution, the optimal pumping field will most likely defy simple intuition. A polyatomic molecule is a complicated quantum-mechanical system, and the external optical forcing field must work cooperatively with the molecular system in order to achieve a physical objective efficiently. Needless to say, the optimality of the excitation strategy obtained by an intuitive procedure is unknown. In an attempt to exploit available analytical and numerical tools, another approach often used is to solve the "forward" problem by determining the response of a given system to various excitations. Examples of such studies can be found in the NMR context[5,6] and in the context of dissociation of polyatomic molecules.[7,8]

The best formulation of such problems should essentially be in the form of an inverse problem, in which the appropriate excitation function or operator that will achieve a given objective is sought. One methodology for treating such problems falls into the domain of optimal control theory.[9,10] It is the purpose of this paper to explore the application of optimal control theory to the excitation of quantum polyatomic molecular systems. The ultimate goal of polyatomic molecular system control will not be examined, but the first rigorous steps will be made. In particular, the mathematical foundations of certain aspects of the quantum-polyatomic control problem are considered, but the numerical illustrations are confined to simpler systems. Although it is impracticable at this stage to numerically treat the large polyatomic excitation problems quantum mechanically, it is still important to consider the optimal control problem for simple quantum systems.

Recently optimal control theory has been applied to the selective excitation problem in NMR (Refs. 11 and 12) and to the design of selective excitation strategies for achieving dissociation in chains of molecules treated both classically[13] and semiclassically.[14] Tannor and Rice[15-17] have used a variational formulation, similar to that used in optimal control, to demonstrate that selectivity of reactivity can be achieved by a two-pulse process: the first pulse is used to excite the molecule; the excited molecule is then allowed to evolve freely and the second pulse is used to stimulate emission, which will bring the molecule back to a desired location on the ground-state potential-energy surface. This approach to selective exci-

tation of a quantum system is quite different from that adopted in this paper where the aim is to design pulses that work cooperatively on the molecular time scale to *actively* steer the system wave packet to its desired objective.

The control of quantum systems has also been investigated from a systems-theoretic point of view. Butkovskii and Samoilenko[18] established a general formalism for the control of quantum systems that applies in a variety of contexts. The controllability of quantum-mechanical systems has also been considered[19,20] and conditions have been derived for the global controllability of quantum systems. A general theory of quantum-dynamical systems with observation, control, and feedback has also been developed.[21,22]

In this paper we consider a specific quantum optimal control problem of achieving, or coming close to, a specified state at a given time. This problem fits into the general framework set out by Butkovskii and Samoilenko[18] and involves the optimal control of a distributed system in which the Schrödinger equation governs the evolution of the state of the system. We consider issues of existence of a solution that require a functional-analytic approach owing to the infinite-dimensional nature of the problem. We also consider the numerical approximation of the optimal control problem and provide some one-dimensional examples. One of the examples provides a model of pulse design for achieving dissociation in a diatomic quantum system. The optimal pulse strategy is shown to exhibit interesting structure that could not be anticipated *a priori*. This study demonstrates the usefulness of a control-theoretic approach to such problems and establishes the well-posedness of is the optimization problem under consideration.

In Sec. II the Schrödinger optimal control problem is formulated and its physical interpretation discussed. In Sec. III we establish the existence of a solution to the proposed optimization problem for external forcing represented by Hilbert-Schmidt operators. We discuss the application of this result in the context of an approximate solution. Although the issue of existence is important to ensure that the problem is well-posed, readers more interested in the physical results may omit Sec. III without loss of continuity. In Sec. IV a Lagrange-multiplier function is used to define a new cost functional and equivalent optimization problem. This new optimization problem is then used to establish necessary conditions for a minimum. These necessary conditions are shown to form the basis for an iterative procedure to search for a minimum. In order to determine a solution to the optimization problem in practical situations, it is necessary to replace the optimization problem by an approximate one over finite-dimensional subspaces of the original function spaces on which the problem was defined. We discuss one such procedure that combines the method of finite differences with a gradient procedure to search for a minimum of the finite-dimensional optimization problem. In Sec. V we illustrate the proposed theory by providing numerical solutions for the control of the one-dimensional Schrödinger equation in which we use the Morse potential to represent a diatomic molecule. Using two different types of excitation, the final state of the quantum system is required to be as close as possible to a variety of specified target states. One such example of particular interest is a model of dissociation in which the final wave packet will eventually leave the bound-potential-well region. Constraints due to the form of the molecular dipole are shown to limit the accessibility of certain types of molecular wave-packet objectives. The effect of the weighting factor used in the definition of the cost functional is also explored.

II. STATEMENT OF THE OPTIMAL CONTROL PROBLEM FOR THE SCHRÖDINGER EQUATION

In this section we formulate the Schrödinger optimal control problem that will be considered in this paper.

Let $\Omega\subset\mathbb{R}^n$ be the spatial domain under consideration and $[0,T]$, the finite interval over which the problem will be posed. We introduce a convenient notation for the Hilbert spaces that will be required in Sec. III:

$$X:=L_2(\Omega),\quad X_t:=L_2(\Omega,[0,T])\ ,$$

$$X':=L_2(\Omega\times\Omega),\quad X_t':=L_2(\Omega\times\Omega,[0,T])\ .$$

The optimal control problem is posed in a standard form[9,10] by considering the minimization of the functional:

$$J[u]=\langle\psi(\cdot,T)-\hat{\psi}(\cdot),\psi(\cdot,T)-\hat{\psi}(\cdot)\rangle_X+\alpha\langle u,u\rangle_{X_t'} \tag{2.1a}$$

subject to

$$i\hbar\frac{\partial\psi}{\partial t}=(H_0+U)\psi\quad\text{for all } x\in\Omega \text{ and } t\in(0,T) \tag{2.1b}$$

and

$$\psi(x,0)=\psi_0(x)\quad\text{for all } x\in\Omega\ .$$

Here $\psi_0,\hat{\psi}\in X$; $H_0:=[-(\hbar^2/2m)\nabla^2+V_0]$ is the Hamiltonian of the quantum system to be controlled, and $\alpha\in\mathbb{R}^+$ is a constant used to balance the relative importance of the terms in the cost functional $J[u]$. All these objects are specified *a priori*. The operator U is defined by

$$U\psi(x,t):=\int_\Omega u(x,x',t)\psi(x',t)dx'\ , \tag{2.1c}$$

where $u(x,x',t)\in X'$ for each t so that U is a Hilbert-Schmidt operator. Conversely, all linear Hilbert-Schmidt operators on X' can be represented in the form (2.1c).[23] Thus a large class of operators can be accommodated in the theory that follows.

Physically the problem (2.1) can be interpreted as finding the external applied forcing (as represented by the operator U) that will make the state ψ as close as possible in the required X norm to the target state $\hat{\psi}$ at time T, while $\|u\|_{X_t'}$ remains finite. The parameter α can be used to prescribe *a priori* the relative importance of the error in achieving the target state $\hat{\psi}$ with respect to the magnitude of the external applied forcing. As an example, in the case where U arises due to an external optical field, the presence of the term $\langle u,u\rangle_{X_t'}$ imposes the require-

ment that the objective $\hat{\psi}$ be reached as best as possible under the constraint of minimal radiative energy deposition.

This formulation provides a quantum-mechanical basis for the more practical task of determining the optimal external force field (e.g., a laser pulse) that has to be applied to a molecule in order to achieve a particular objective such as dissociation of selected atoms from the molecule.

III. EXISTENCE OF AN OPTIMAL SOLUTION TO THE SCHRÖDINGER CONTROL PROBLEM

In this section we establish the existence of a solution to the optimization problem (2.1).

Theorem 1. There exists a solution $\tilde{u} \in U_{\text{ad}} = \{u : u \in X_t'\}$ (the space of admissible controllers) and a corresponding $\tilde{\psi} \in X_t$ that solves the optimization problem (2.1).

Proof. By the definition of the infimum there exists a sequence $\{u_n\}$ of functions in U_{ad} such that

$$\lim_{n\to\infty} J[u_n] = \inf_{u\in U_{\text{ad}}} J[u] . \tag{3.1}$$

Claim 1. The sequence $\{u_n\}$ defined in (3.1) is uniformly bounded in n.

Proof. By contradiction. Assume that there exists a subsequence $\{u_{n_k}\}$, such that given any $M>0$ there exists an N for which

$$n_k > N \Longrightarrow M < \|u_{n_k}\|_{X_t'} .$$

However, $J[u_{n_k}] \to \infty$ as $\|u_{n_k}\|_{X_t'} \to \infty$ which contradicts the construction $\{u_n\}$ given in (3.1). Thus there exists an $M>0$:

$$\|u_n\|_{X_t'} \le M \quad \text{for all } n . \qquad \text{QED}$$

Claim 2. The sequence $\{\psi_n\}$ of solutions to (2.1b) and (2.1c) that correspond to $\{u_n\}$ is uniformly bounded in n.

Proof. We consider in this paper potentials V_0 for which H_0 generates a C_0 semigroup $S_{H_0}(t)$ on X.[24] Let $\{U_n\}$ denote the sequence of operators associated with $\{u_n\}$ by means of (2.1c). Considering U_n as a bounded perturbation to H_0 it can be shown[24] to generate a C_0 semigroup $S_{H_0+U_n}(t)$ with the following property:

$$\|U_n\|_{\text{op}} \le M_n ,$$

$$\|S_{H_0}(t)\|_{\text{op}} \le c e^{\omega t} \Longrightarrow \|S_{H_0+U_n}(t)\|_{\text{op}} \le c e^{(\omega+M_n)t} .$$

Now by the definition of the semigroup,

$$\psi_n(\cdot,t) = S_{H_0+U_n}(t)\psi_0(\cdot) .$$

We combine this representation with claim 1, which ensures the existence of an $M>0$, $M_n<M$ for all n, with the above estimate on the semigroup $S_{H_0+U_n}$ to obtain

$$\|\psi_n(\cdot,t)\|_X \le c' e^{(\omega+M)t} .$$

Squaring and integrating over $[0,T]$ we obtain the result

$$\|\psi_n\|_{X_t} \le c'' . \qquad \text{QED}$$

Since the closed unit ball is weakly compact in a Hilbert space,[25] it follows from claim 1 that there exists a subsequence $\{u_{n_k}\}$ of $\{u_n\}$ that converges weakly in U_{ad}, so that

$$u_{n_k} \overset{\text{weak}}{\to} \tilde{u} \quad \text{as } k\to\infty .$$

Now since a Hilbert space is weakly closed, $\tilde{u} \in U_{\text{ad}}$. Similarly, applying claim 2 to the corresponding subsequence $\{\psi_{n_k}\}$ we can establish that there exists a weakly convergent subsequence of $\{\psi_{n_k}\}$ in X_t which converges to an element $\tilde{\psi} \in X_t$. Thus taking the intersection of all these subsequences we obtain two sequences:

$$\{u_s\}: \lim_{s\to\infty} u_s = \tilde{u} \in U_{\text{ad}} ,$$

$$\{\psi_s\}: \lim_{s\to\infty} \psi_s = \tilde{\psi} \in X_t ,$$

where the limits are weak limits, and ψ_s is the solution of (2.1b) and (2.1c) corresponding to u_s. We now show that $\tilde{u}$ is the minimizer:

$$\begin{aligned} J[\tilde{u}] = J\left[\lim_{s\to\infty} u_s\right] &= \left\langle \lim_{s\to\infty}\psi_s, \lim_{s\to\infty}\psi_s \right\rangle_X - \left\langle \hat{\psi}, \lim_{s\to\infty}\psi_s \right\rangle_X - \left\langle \lim_{s\to\infty}\psi_s, \hat{\psi} \right\rangle_X + \alpha \left\langle \lim_{s\to\infty} u_s, \lim_{s\to\infty} u_s \right\rangle_{X_t'} + \langle \hat{\psi}, \hat{\psi} \rangle_X \\ &= \left\langle \lim_{x\to\infty}\psi_s, \lim_{s\to\infty}\psi_s \right\rangle_X - \lim_{s\to\infty} \langle \hat{\psi}, \psi_s \rangle_X - \lim_{s\to\infty} \langle \psi_s, \hat{\psi} \rangle_X + \alpha \left\langle \lim_{s\to\infty} u_s, \lim_{s\to\infty} u_s \right\rangle_{X_t'} + \langle \hat{\psi}, \hat{\psi} \rangle_X \end{aligned}$$

by the definition of weak convergence. (All limits in angular brackets are weak limits.) We have

$$\begin{aligned} J[\tilde{u}] &\le \lim_{s\to\infty} \inf \|\psi_s\|_X^2 - \lim_{s\to\infty} \langle \hat{\psi}, \psi_s \rangle_X - \lim_{s\to\infty} \langle \psi_s, \hat{\psi} \rangle_X \\ &\quad + \alpha \lim_{s\to\infty} \inf \|u_s\|_{X_t'}^2 + \|\hat{\psi}\|_X^2 \\ &= \inf_{u\in U_{\text{ad}}} J[u] , \end{aligned}$$

using the weak lower semicontinuity of the inner product. Thus we have proved the existence of an element $\tilde{u} \in U_{\text{ad}}$ that achieves the infimum value of J on U_{ad}. This proves the theorem.

Comment. It is of interest to consider the case in which the operator U defined in (2.1c) corresponds to multiplication by some function. The operator U would then represent an external applied potential. This could be represented formally by letting $u(x,x',t) = \delta(x$

$-x')u(x',t)$ in (2.1c). However, in this case $u \notin X'$; so theorem 1 does not apply. If we replace the δ function by a δ-sequence function δ_ϵ so that $u_\epsilon(x,x',t)=\delta_\epsilon(x-x')u(x',t)$, then theorem 1 does apply and there exists a solution to the optimization problem for each $\epsilon>0$. This is all that we require from the point of view of an approximate solution of the optimization problem, as δ_ϵ can be chosen to be much narrower than the physical length scale of the problem, and the operator U can be replaced by the multiplicative factor $u(x,t)$. In the remainder of this paper we consider operators of a multiplicative form in the context of an approximate solution.

IV. LAGRANGE-MULTIPLIER FORM OF THE OPTIMAL CONTROL PROBLEM, NECESSARY CONDITIONS FOR A MINIMUM, AND APPROXIMATE SOLUTION

In this section we reformulate the optimization problem (2.1) using a Lagrange-multiplier function. We derive necessary conditions for a minimum and discuss the approximate solution of the optimization problem. We assume that U is in the form of a multiplication operator so that it may be interpreted as an external applied potential. Theoretical justification for this assumption is discussed in the comment at the end of Sec. III.

A. Lagrange-multiplier formulation

Let $p(x,t)\in X_t$ and consider the minimization problem: Find $\tilde{u}$, $\tilde{\psi}$, and $\tilde{p}$:

$$L[\tilde{u},\tilde{\psi},\tilde{p}]=\inf_{\substack{u\in X_t\\ \psi\in X_t^0\\ p\in X_t}} L[u,\psi,p]\ , \tag{4.1}$$

where

$$L[u,\psi,p]:=J[u]+\mathrm{Re}\int_0^T\int_\Omega p\left[\dot{\psi}+\frac{i}{\hbar}(H_0+u)\psi\right]^* dx\,dt$$

and

$$X_t^0=X_t\cap\{\psi:\psi(x,0)=\psi_0(x)\}\ .$$

The introduction of the term with the Lagrange multiplier assures that the Schrödinger equation is satisfied at the minimum of the functional.

B. Necessary conditions

Necessary conditions for a minimum are obtained by taking the Fréchet derivatives of $L[u,\psi,p]$ with respect to the argument functions u, ψ, and p and equating them to zero:

$$0=\frac{\delta L}{\delta p}\delta p\Longrightarrow\dot{\tilde{\psi}}=-\frac{i}{\hbar}(H_0+u)\tilde{\psi},\quad \tilde{\psi}(x,0)=\psi_0(x)\ , \tag{4.2a}$$

$$0=\frac{\delta L}{\delta\psi}\delta\psi\Longrightarrow\dot{\tilde{p}}=-\frac{i}{\hbar}(H_0+u)\tilde{p}\ ,$$
$$\tilde{p}(x,T)=2[\hat{\psi}(x)-\tilde{\psi}(x,T)]\ , \tag{4.2b}$$

$$0=\frac{\delta L}{\delta u}\delta u\Longrightarrow 0=\int_0^T\int_\Omega\left[2\alpha\tilde{u}-\mathrm{Re}\left[\tilde{p}\frac{i}{\hbar}\tilde{\psi}^*\right]\right]\delta u\,dx\,dt\ . \tag{4.2c}$$

The necessary conditions for a minimum (4.2a)–(4.2c) form the basis for an iterative procedure that starts with a trial applied potential $u^{(0)}$ from which the corresponding solutions $\psi^{(0)}$ and $p^{(0)}$ can be found using (4.2a) and (4.2b), respectively. These functions can then be used to compute the gradient $\delta L/\delta u$. This gradient is then used to identify a search direction to look for a new applied potential $u^{(1)}$ for which the value of L is lower. Since this search is infinite dimensional, we shall for practical purposes replace the Hilbert spaces X, X_t, and X_t^0 by finite-dimensional subspaces on which the optimization problem is posed. The corresponding necessary conditions yield a search procedure on the finite-dimensional subspaces, and the gradient can be used to search for an optimal applied potential by the method of steepest descents or by a conjugate direction procedure.[26]

C. Approximate solution

Thus far all the results in this paper are general in that the quantum control system could contain an arbitrary number of particles in three spatial dimensions. We now restrict our discussion here to problems involving the numerical solution of the Schrödinger equation (2.1b) in one spatial dimension. The procedure can be extended directly to higher dimensions, neglecting for the moment the concomitant computational burden of such an extension.

Given a trial potential $u^{(k)}$ we solve (4.2a) and (4.2b) numerically using finite differences.[27] For the one-dimensional problem in which $\Omega=[0,L]$ we divide the spatial domain into N equal subintervals of length $\Delta x=L/N$. The mesh points formed by the end points of these subintervals are denoted by $x_n=n\Delta x$ and the numerical solution at such a mesh point is denoted by $\psi_n^{(k)}(t)\approx\psi^{(k)}(x_n,t)$. We now approximate the operator $H=H_0+u$ using central differences so that (4.2a) is approximated by

$$\dot{\psi}_n^{(k)}=-\frac{i}{\hbar}H_n^{(k)}(t)\psi_n^{(k)}\ , \tag{4.3}$$

where

$$H_n^{(k)}(t):=\{-q\underline{E}+[V_{0,n}+u_n^{(k)}(t)+2q]\underline{I}-q\underline{E}^{-1}\}\ .$$

Here $q=\hbar^2/2m\Delta x^2$, $\underline{E}$ is the spatial shift operator defined by $\underline{E}\psi_n=\psi_{n+1}$, and $\underline{I}$ is the identity operator.

In order to solve the system of ordinary differential equations (ODE's) (4.3) we use the Crank-Nicholson procedure.[27] The time interval $[0,T]$ is divided into J subintervals of length $\Delta t=T/J$. The end points of these subintervals are denoted by $t_j=j\Delta t$, and superscripts are used to denote the time step at which a quantity is evaluated, i.e., $\psi_n^j\approx\psi(x_n,t_j)$. The Crank-Nicholson procedure can now be expressed in the form

$$\left[I+i\frac{\Delta t}{2\hbar}H_n^{(k),j+1}\right]\psi_n^{(k),j+1}=\left[I-\frac{i\Delta t}{2\hbar}H_n^{(k),j}\right]\psi_n^{(k),j}\ . \tag{4.4}$$

Since $\psi_n^{(k),0}=\psi_0(x_n);n=0,\ldots,N$ the numerical solution $\{\psi_n^{(k),j}\}_{n=0,\ldots,n}^{j=0,\ldots,J}$ can be found by a marching process using (4.4), which involves an inversion of the tridiagonal matrix $[I+(i\Delta t/2\hbar)H_n^{(k),j+1}]$ at each time step.

The reason for choosing the implicit Crank-Nicholson procedure in preference to an explicit scheme such as the "leapfrog" method[28] is that for explicit schemes the bound on the time step Δt depends on the unknown applied potential $u(x,t)$. Thus it is impossible to determine *a priori* the magnitude of the time steps Δt. The Crank-Nicholson scheme has a stability region $\mathrm{Re}(z)\leq 0$, and since the eigenvalues of the Toeplitz operator $(i/\hbar)H_n(t)$ lie along the imaginary axis we conclude that the difference scheme (4.4) is unconditionally stable. The Crank-Nicholson scheme can be shown[28] to conserve the probability density in that $(\psi^{j+1},\psi^{j+1})=(\psi^j,\psi^j)$.

A similar procedure is used to determine the approximate Lagrange-multiplier function $\{p_n^{(k),j}\}_{n=0,\ldots,N}^{j=0,\ldots,J}$ from (4.2b), in this instance marching backward in time.

We assumed above that $u_n^{(k),j}$ was known, and calculated the associated $\psi_n^{(k),j}$ and $p_n^{(k),j}$. All these can now be used to determine the gradient derived from (4.2c):

$$G_n^{(k),j}=\left[2\alpha u_n^{(k),j}-\mathrm{Re}\left[p_n^{(k),j}\frac{i}{\hbar}\psi_n^{(k),j*}\right]\right]\omega_n^j\Delta x\,\Delta t\ ,$$

where ω_n^j are some appropriately chosen numerical quadrature weights. The method of steepest descent[26] can now be used to determine a new approximate applied potential

$$u_n^{(k+1),j}=u_n^{(k),j}-\beta^{(k)}G_n^{(k),j}\ ,$$

where $\beta^{(k)}$ is a non-negative scalar minimizing $J[u_n^{(k),j}-\beta G_n^{(k),j}]$. Naturally the gradient $G_n^{(k),j}$ can also be used to set up a conjugate direction search procedure such as the Polak-Rabiere method.[26]

V. NUMERICAL RESULTS

A. Introduction

In this section we illustrate the above theory in the particular case of controlling the Schrödinger equation in one spatial dimension. We assume that U is in the form of a multiplicative operator; therefore, it may be interpreted as an external applied potential. Theoretical justification for this assumption is discussed in the comment at the end of Sec. III. In this case (2.1b) can be written in the form

$$i\hbar\frac{\partial\psi}{\partial t}=\left[-\frac{\hbar^2}{2m}\frac{\partial^2}{\partial x^2}+V_0(x)+u(x,t)\right]\psi\ . \tag{5.1}$$

We also choose V_0 to be the Morse potential,

$$V_0(x)=D(1-e^{-\gamma(x-x_0)})^2\ , \tag{5.2}$$

which represents the potential-energy function of a diatomic molecule. This simple example suffices to illustrate the possibility of molecular control, while more realistic cases must await further numerical calculations.[13,14]

In keeping with the formulation presented earlier in the paper, the objective in each of the examples will be a particular wave-function shape $\psi(x,T)$ at a chosen time T. Although steering wave packets to target shapes does not correspond to an actual laboratory observable, the ability to steer wave packets ultimately provides the freedom to attain any other meaningful objectives. In addition, the choice of T should not be viewed as a critical matter since in real molecular control problems it may be made sufficiently large so as to insure insensitivity to its value and convergence of the optical pulse shape in a laser control problem.[13,14]

In order to reduce (5.1) to a dimensionless form, we rescale the length according to $x=\delta X$. We choose $\delta=(\hbar/m\omega)^{1/2}$, where $\omega=\gamma(2D/m)^{1/2}$ is the frequency of the harmonic oscillator associated with (5.2) for $|X-X_0|\ll 1$. In this case (5.1) and (5.2) yield

$$\frac{i}{\omega}\frac{\partial\psi}{\partial t}=\left\{-\frac{1}{2}\frac{\partial^2}{\partial X^2}+\frac{N}{2}\left[1-\exp\left[-\frac{X-X_0}{N^{1/2}}\right]\right]^2+u(X;t)\right\}\psi(X,t)\ , \tag{5.3}$$

where $N=2D/\hbar\omega$ is the maximum number of bound states, and $u(\delta X,t)/\hbar\omega$ is replaced by the dimensionless applied potential $u(X,t)$. In all the numerical examples presented in this section we assume $\omega=1$ and $N=10$. Throughout this section we shall consider control over a time interval $[0,T]$ in which $T=8\pi$ or four periods of oscillation at the fundamental frequency $\omega=1$.

In the numerical experiment described below we consider the following.

(1) Two different types of external applied potentials: (P1), $u(X,t)=B(X)E(t)$, where $B(X)$ is a specified dipole function, e.g., linear in X; and (P2), $u(X,t)$, an arbitrary function of X and t. The potential (P1) is realistic since it represents the external potential due to a dipole moment $B(X)$ subjected to a time-varying electric field $E(t)$. The electric field $E(t)$ is to be determined by the optimization procedure. Since the potential (P2) has more freedom than (P1) we can expect a lower minimum of J to be achieved than for the more constrained case (P1). The potential (P2) may not be realized in the laboratory, but it is interesting to consider for its contrasting behavior to the spatially constrained case.

(2) A variety of different values of the parameter α: This parameter in (2.1) and (4.1) determines the relative importance in the cost functional $J[u]$ of the error in achieving the target state $\hat{\psi}$ compared to the magnitude of the external applied forcing. If $0<\alpha\ll 1$, then we are allowing the external field to be essentially as large as necessary to achieve the target $\hat{\psi}$. Naturally there exists a critical range of values of α in which the two terms in the cost functional are balanced, and the optimization routine makes a direct trade between achieving the target and increasing the magnitude of the external forcing. If α is made still larger, then the external forcing can no longer influence the state appreciably. An alternative to choosing the parameter α would be to place a constraint on $\|u\|_{X_t}$ directly. This constrained optimization problem is not considered here, but it would be appropriate if

there were some practical limitation placed on $\|u\|_{X_t}$ (e.g., if field intensities of only a specific bounded value could be achieved).

(3) Gaussian target wave packets $\hat{\psi}(x)$: These we position at various places in the interval $[0,L]$. We formulate a model of dissociation within the context of the optimal-control problem (2.1) by requiring that the position of the target wave packet be such that the expectation value of the Hamiltonian is sufficient for dissociation (assuming that significant spontaneous energy loss does not occur during the subsequent unforced free wave-packet evolution).

B. Translating a Gaussian wave packet

The numerical results in this subsection have been chosen to demonstrate that it is indeed possible to determine an external applied potential that will result in a specified target wave packet being achieved at a given time $T=8\pi$. We consider the two types of external applied potentials (P1) and (P2) discussed in Sec. V A, and the results for these optimally determined external potentials are given in Figs. 1 and 2, respectively.

In this calculation the domain extends from 0 to $L=16.0$ and the bottom of the potential well is at $X_0=4.0$. We define the function

$$g(\xi,\xi_0,l)=\pi^{-1/4}l^{-1/2}\exp[-(\xi-\xi_0)^2/2l^2] \tag{5.4}$$

and choose the initial wave function to be $\psi_0(X)=g(X,X_0=4,1)$, and the target state to be the same Gaussian centered at $X_f=8.0$, so that $\hat{\psi}(X)=g(X,8,1)$. For the spatially constrained dipole function (P1) we choose $B(X)=-(X-X_0)$ with unit magnitude transition dipole. For both potentials (P1) and (P2) the value of α is 10^{-7}, so effectively we allow the magnitude of the potential to become as large as is required.

Comparing Figs. 1(a) and 2(a) we notice that there is a closer correspondence between the final state $\hat{\psi}(X,T)$ and the target state $\psi(X)$ for (P2) (the external field with full freedom) than for (P1) (the external potential constrained to be a linear function of X). This is to be expected from an optimization point of view, as we are minimizing over a smaller space of functions in the constrained case and one would therefore expect the minimum achieved to be larger. However, what is of more importance is the interpretation in terms of controllability since the spatially constrained field is less able to control the state. In terms of achieving the objective, this phenomenon demonstrates the limitation that results from placing a physical constraint on the spatial variation of the controller. This limitation could in principle be alleviated to some degree by nonlinear feedback to the dipole function through coherent modification of the molecular electronic structure for sufficiently intense electric fields.

The nature of the reduced correspondence between the final state and the target state in the case of the constrained external potential (P1) is also significant. In this case the final wave packet is broader than the desired target. This can be explained by observing that the external applied potential $-(X-X_0)E(t)$ pivots [see Fig. 1(b)] about the point X_0 and that the gradient of the potential $V_0(X)$ decreases as X increases away from X_0. As a result, an enhanced effective instantaneous curvature of the combined potential $V_0(X)-(X-X_0)E(t)$ cannot be achieved in the region $X>X_0$ by any value of $E(t)$. This limitation is illustrated graphically in Fig. 1(c) in which the initial potential $V_0(X)$, the applied potential corresponding to the maximum value $E_{\max}$ of $E(t)$, and the net potential $V_0(X)+B(X)E_{\max}$ are plotted. We see that in the target region $X=8.0$ the curvature of the net potential is, in fact, negative. This causes the spreading in the final wave packet observed in Fig. 1(a), and demonstrates that sharpening or even direct translation of the wave packet is difficult to achieve in the region $X>X_0$ using this particular spatially constrained controller. Even the location of the dipole zero, $X=X_0$ in this case, will also influence the effectiveness of the constrained field.

One way of modeling dissociation (see Sec. V D below for further discussion) using the optimal control formulation (2.1) would be to specify a target wave packet $\hat{\psi}(x)$ that is sufficiently narrow that the target energy $\mathcal{E}=\langle\hat{\psi},H_0\hat{\psi}\rangle$ is larger than the dissociation energy of 5.0. The spreading phenomenon described above implies that it would be difficult to try to sharpen the wave packet in the region $X>X_0$ by means of a spatially constrained controller of the form $-(X-X_0)E(t)$. This difficulty was verified numerically and indicates that an inherent limitation in the molecular Hamiltonian H_0 or the dipole function $B(X)$ can make certain objectives unattainable.

In Fig. 1(d) the plot of $E(t)$ is positioned above the space-time contour plot of the corresponding probability density $|\psi(X,t)|^2$. The function $E(t)$ is proportional to the section through the surface $B(X)E(t)$ at $X=16.0$ in Fig. 1(b). The response of the wave packet can be seen to lag behind the larger peaks of $E(t)$ by a factor of approximately $\pi/2$. In this example, as well as all the others, the field structure reflects knowledge of where the wave packet is currently located and where it is going. This is brought about by the feedback process carried through the Lagrange-multiplier function $p(X,t)$. The strategy of the spatially constrained controller $B(X)E(t)$ is essentially to exploit the walls of the potential to guide the wave packet to the final target position. This can be seen by the two large-amplitude pulses at $t=\pi$ and 6π. Between these two pulses there is an interval of comparitively low-amplitude, higher-frequency phase adjustment. The excitation that occurs at the end of the time interval between 6π and 8π is essentially a low-frequency pulse at about the fundamental frequency $\omega=1$. The contour plot in Fig. 1(d) illustrates that the wave packet is not spatially dispersed during the time period $[0,T]$. The response to the low-amplitude, higher-frequency phase adjustment is in the form of the closely distributed (in space and, time respectively) peaks that occur between 2π and 5π. The fact that the field $E(t)$ is not identically zero at $T=8\pi$ can be explained by observing that we specified that the wave packet shall be at rest at $T=8\pi$. Thus there is a very short deceleration period at the end of the interval $[0,T]$. In Fig. 1(e) it can be seen that the power

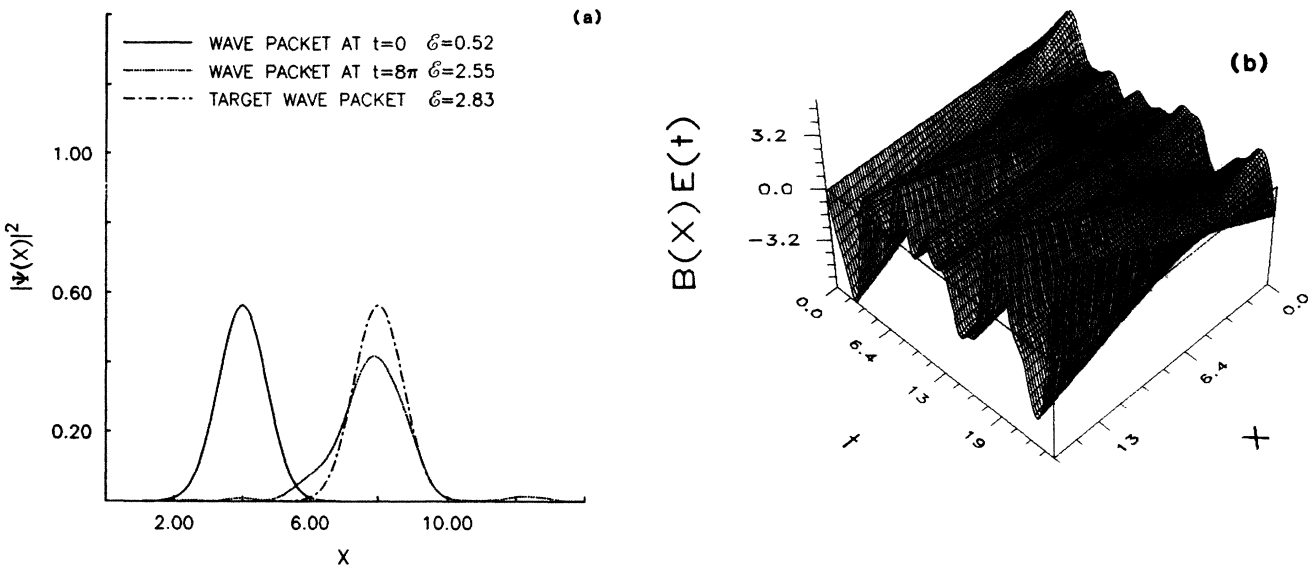

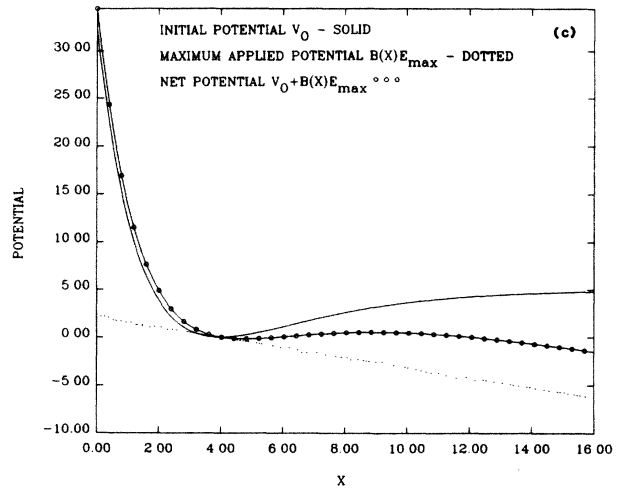

FIG. 1. A Gaussian wave packet translated from $X_0=4.0$ to $X_f=8.0$ by a spatially constrained external applied potential (P1) $B(X)E(t)=-(X-X_0)E(t)$. (a) The probability densities of the initial wave packet $\psi_0(X)$, the final wave packet $\psi(X,T)$ achieved using $B(X)E(t)$, and the target wave packet $\hat{\psi}(X)$. (b) The external applied potential $B(X)E(t)$ over the space-time domain $[0,16.0]\times[0,8\pi]$. At any instant of time the spatial form of this external potential is a linear ramp of positive or negative slope. This alternating ramp, when combined with the Morse potential $V_0(X)$, provides the control for guiding the wave packet to the desired final objective. (c) The Morse potential $V_0(X)$, the applied potential corresponding to the maximum value $E_{\max}$ of $E(t)$, and the net potential $V_0(X)+B(X)E_{\max}$. The negative curvature of the net potential in the target region $X=8.0$ explains the spreading of the final wave packet shown in (a). (d) The plot of the electric field $E(t)$ over the time interval $[0,8\pi]$ is positioned above the contour plot of the probability density $|\psi(X,t)|^2$ over the space-time domain $[0,16]\times[0,8\pi]$ so that the time intervals are aligned. The response of the wave packet to the driving electric field can be observed. The field tends to lead the wave packet by a time period of approximately $\pi/2$. There are two pulses at $t=\pi$ and 6π which are low frequency and have relatively large amplitudes. Between these two pulses there is a stage of higher-frequency phase adjustment. (e) The power spectrum of $E(t)$, i.e., the magnitude of the discrete Fourier transform normalized to unity. The rightmost peak corresponds to the fundamental frequency $\omega=1.0$. The occurrence of some higher-frequency components with lower amplitudes is consistent with the phase adjustment stage. (f) The energy $\mathcal{E}(t)$ of the wave packet over the time interval $[0,8\pi]$. The electric field $E(t)$ is superimposed on this plot (see dashed curve). The correspondence between the larger-amplitude pulses in $E(t)$ and the deposition of energy to the molecular wave packet can be observed. All the quantities used in this figure are dimensionless.

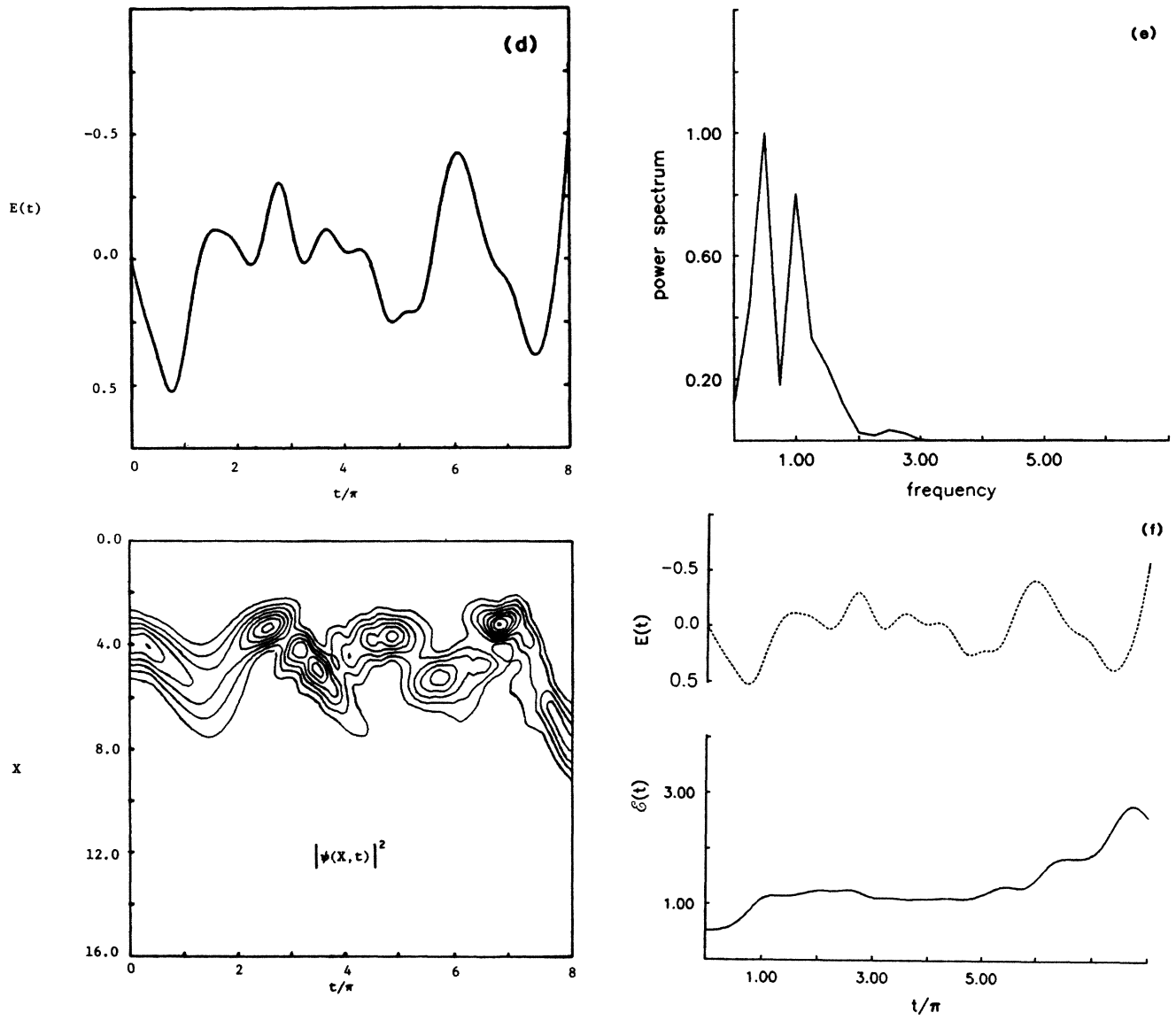

FIG. 1. (*Continued*).

spectrum of $E(t)$ contains some low-amplitude, high-frequency components, but the low-frequency components dominate the spectrum. The second peak centered at a frequency of 1.0 corresponds to the fundamental frequency of the Morse oscillator. This information is consistent with the phase adjustment interval, followed by the low-frequency pulsing toward the end of the time interval that we observed above.

In Fig. 1(f) the time evolution of the energy of the wave packet is plotted. Superimposed on this plot is the applied field $E(t)$. The phase adjustment excitation does little to the energy of the wave packet, whereas the three main jumps in energy can be seen to correspond directly to the large-amplitude low-frequency pulsing. The drop in energy at the end of the time interval corresponds to the deceleration phase to bring the wave packet to rest at $T=8\pi$ in order to match the target wave packet.

As can be seen from Fig. 2(b) the strategy of the controller (P2) with full freedom is far more complicated than the spatially constrained controller (P1). In Fig. 2(c) we juxtapose: the diagram showing positive (dark shading) and negative (light shading) regions of $u(X,t)$, the space-time contour plot of the probability density $|\psi(X,t)|^2$, and the positive (dark shading) and negative (light shading) regions of the probability flux vector $\mathbf{J}:=(\hbar/m)\mathrm{Im}(\psi^*\nabla\psi)$. The nature of the field $u(X,t)$ does not allow direct comparison between the constrained (P1) and unconstrained controller (P2). However, a qualitatively similar interpretation can be given to the unconstrained controller (P2) if we regard the duration time of the moving valleys (light shading) in Fig. 2(c) (i) as a measure of the period of oscillation. Interpreted thus, a high-frequency phase adjustment stage between $t=0$ and 4π can be identified. In response, the wave packet is both dispersed and concentrated in rapid succession within this interval. This is strikingly demonstrated by the small regions of alternating flux of short duration that occur in the interval $[0,4\pi]$.

The low-frequency excitation toward the end of $[0,T]$, which was a feature of the spatially constrained controller (P1), also has its counterpart in this setting of control with full freedom (P2). In the interval $[4\pi,8\pi]$ the wave packet is *guided* to the target position by a local deepening well of long duration indicated by the dashed line in Fig. 2(c) (i). This local well is flanked by high but localized walls that serve to concentrate the wave packet with a view to achieving the final target state. The large uninterrupted regions of probability flux shown in Fig. 2(c) (iii) confirm the observation that the probability amplitude is being channeled to achieve the final target state. The dashed line marking the bottom of the guiding well shown in Fig. 2(c) (i) has also been superimposed on the wave-packet contour plot shown in Fig. 2(c) (ii). As was the case with the spatially constrained controller (P1), the wave packet in this case of full control (P2) also exhibits a phase lag relative to the controller.

In Fig. 2(d) the time evolution of the energy $\mathcal{E}(t)$ of the wave packet is plotted. The energy increase for the unconstrained controller (P2) is far more uniform than for the constrained controller (P1). In the case (P2) the energy increases monotonically, unlike the spatially constrained controller (P1), which transfers small amounts of energy back to the applied field.

As a measure of the *average* energy involved in applying an external potential $u(X,t)$ we define the functional

$$\mathcal{E}[u]:=\frac{1}{T}\int_0^T\int_\Omega |\psi(X,t)|^2\,|u(X,t)|\,dX\,dt\ . \tag{5.5}$$

In the case of the potential $u(X,t)$ with full freedom,

$$\mathcal{E}[u]=0.10\ ,$$

whereas for the spatially constrained external potential,

$$\mathcal{E}[BE]=0.25\ .$$

Thus the energy required of the spatially constrained field is somewhat higher than that required of the unconstrained field. This is also true of the maximum applied field values, since $\|u\|_\infty=0.5$, whereas $\|BE\|_\infty=6.3$. These latter numbers may be compared to the potential well depth $N/2=5.0$, and in the constrained case it is evident that the applied field is quite strong. In realistic problems care will be required to ensure that significant electronic disturbances do not also occur. As mentioned above, this possibility could be turned into an asset if it could be treated in the cost functional $J[u]$.

C. The effect of the weighting factor α

In this subsection we explore the effects of the parameter α that balances the two terms in the cost functional

$$J[u]=\|\psi-\hat{\psi}\|_X^2+\alpha\|u\|_{X_t}^2\ .$$

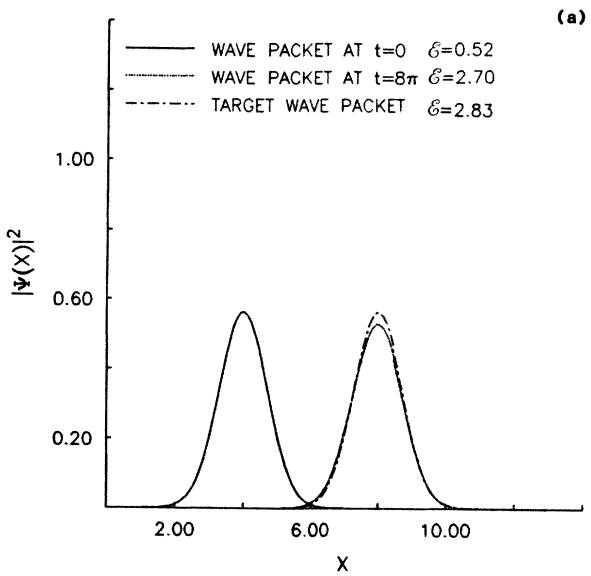

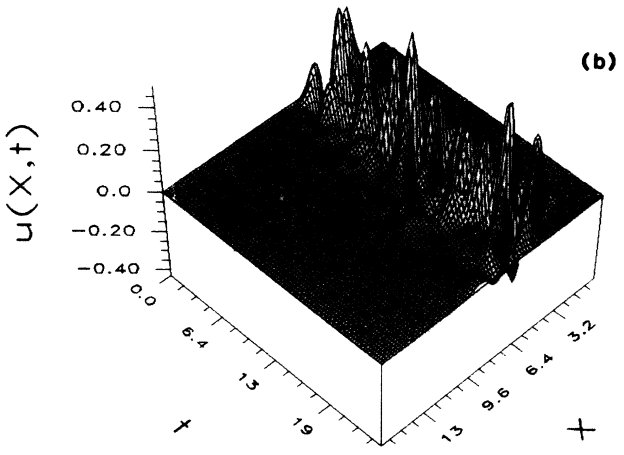

FIG. 2. A Gaussian wave packet translated from $X_0=4.0$ to $X_f=8.0$ by an unconstrained applied potential (P2) $u(X,t)$. (a) The probability densities of the initial wave packet $\psi_0(X)$, the final wave packet $\psi(X,T)$ achieved using $u(X,t)$, and the target wave packet $\hat{\psi}(X)$. (b) The external applied potential $u(X,t)$ over the space-time domain $[0,16.0]\times[0,8\pi]$. The spatially localized, complex structure of this potential should be contrasted with that of the constrained potential shown in Fig. 1(b). (c) Three space-time plots with an aligned time interval. (i) Regions of positive (dark shading) and negative (light shading) applied potential $u(X,t)$. (ii) A contour plot of the probability density $|\psi(X,t)|^2$ with contour intervals $\Delta|\psi|^2=0.1$. (iii) Positive and/or negative regions of the flux vector $\mathbf{J}(X,t)$. The positive regions (dark shading) represent regions in which there is a flux of material in the positive-X direction, whereas negative regions (light shading) represent regions in which the flux of material is in the negative-X direction. A similar period to that of Fig. 1 of high-frequency phase adjustment can be observed. This is followed by a stage in which the wave packet is guided to the objective by a deepening well indicated by the dashed line. The same dashed line on the contour plot of the probability density demonstrates the phase lag of the wave packet behind the external excitation. The large uninterrupted regions of material flux confirm that the wave packet is being chanelled to the final state toward the end of the interval $[0,8\pi]$. (d) The energy $\mathcal{E}(t)$ of the wave packet over the time interval $[0,8\pi]$. In this case the energy absorption of the wave packet is monotonic, which was not the case for the spatially constrained controller [see Fig. 1(f)]. All the quantities used in this figure are dimensionless.

Three regions of values of α can be identified by the ratio $R=\|\tilde{\psi}-\hat{\psi}\|_X^2/\alpha\|\tilde{u}\|_{X_t}^2$ where $\tilde{u}$ is the control in the limit $\alpha\to 0$.

(i) $R\gg 1$. In this case field energy is unrestricted and the only limitation on the controller originates from the reachability of the molecular objective by the class of controller being considered.

(ii) $R=O(1)$. A direct tradeoff has to be made between decreasing $\|\psi-\hat{\psi}\|_X^2$ and the associated increase in $\|u\|_{X_t}^2$.

(iii) $R\ll 1$. In this case essentially all the effort will go to decreasing $\|u\|_X^2$ and a poor match between ψ and $\hat{\psi}$ can be expected.

Depending on the purpose of the control problem, an appropriate choice of α has to be made so that $J[u]$ should operate in the appropriate regions (i), (ii), or (iii). A factor to consider may also be unwanted damage (e.g., electronic disturbance) to the target molecule or others in the medium, but we do not consider such cases here.

We now consider the translated Gaussian wave-packet problems of Sec. V B with a range of values of α. Figure 3 compares the probability distributions $|\psi(X,T)|^2$ of three final states for the spatially constrained field (P1) using the values (i) $\alpha=10^{-7}$, (ii) $\alpha=10^{-3}$, and (iii) $\alpha=10^{-2}$. The degradation in performance can be seen clearly in Fig. 3 while the energy of the controller in each case is (i) $\mathcal{E}[BE]=0.25$, (ii) $\mathcal{E}[BE]=0.05$, and (iii) $\mathcal{E}[BE]=0.03$. In Fig. 3(b) $E(t)$ is plotted for comparison in each of the three cases. As α increases, not only is there the expected lowering of amplitude of $E(t)$, but the field also does not make the important small higher-frequency phase adjustments seen in the case $\alpha=10^{-7}$. Figure 4 compares the probability distributions $|\psi(X,T)|^2$ of three distinct final states that are obtained using the values (i) $\alpha=10^{-7}$, (ii) $\alpha=10^{-1}$, and (iii) $\alpha=1$, and for the potential (P2) with full freedom $u(X,t)$. The degradation in performance can be seen clearly in Fig. 4, while the average energy associated with the controller in each case is (i) $\mathcal{E}[u]=0.12$, (ii) $\mathcal{E}[u]=0.11$, and (iii) $\mathcal{E}[u]=0.07$.

The above results demonstrate how the value of the parameter α implicitly affects the emphasis of the terms in the cost functional $J[u]$. Depending on the objective of the control problem, the emphasis can be placed on reducing the energy of interaction rather than reducing the error in matching the target, or vice versa. In some

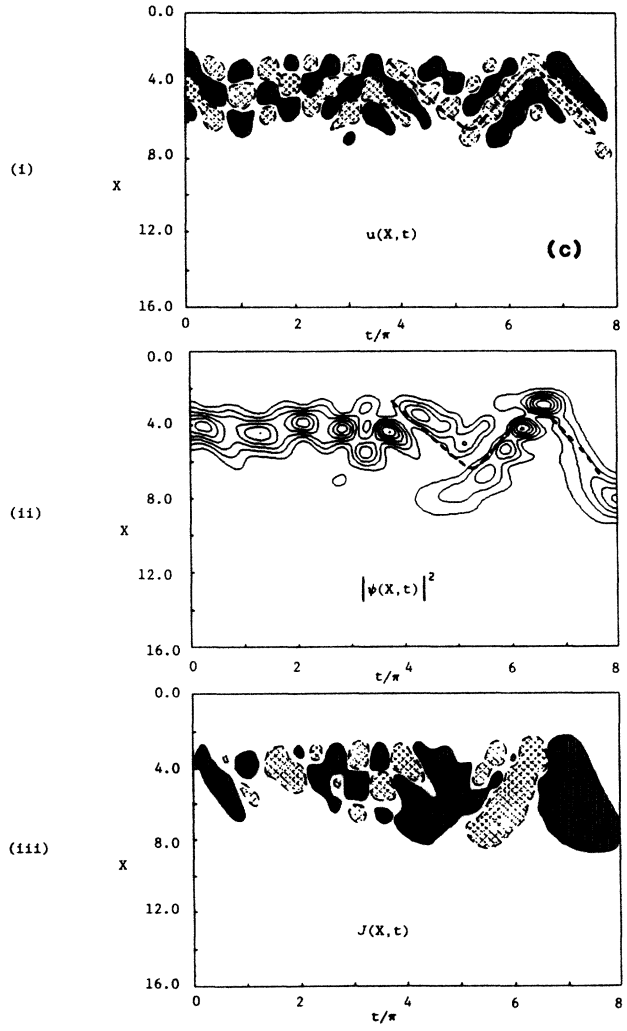

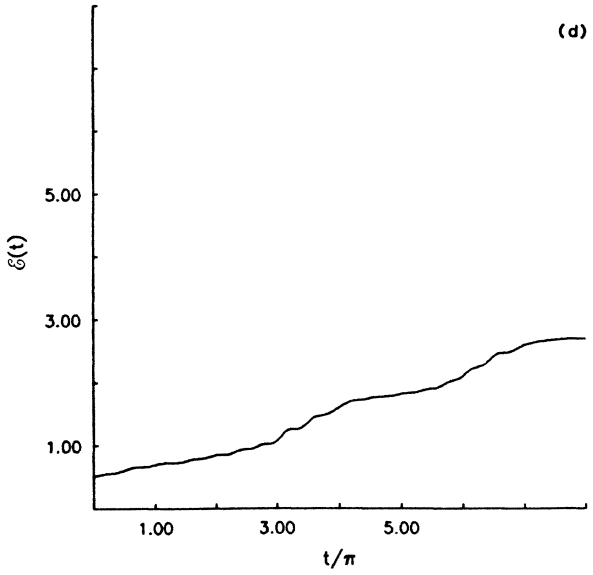

FIG. 2. (*Continued*).

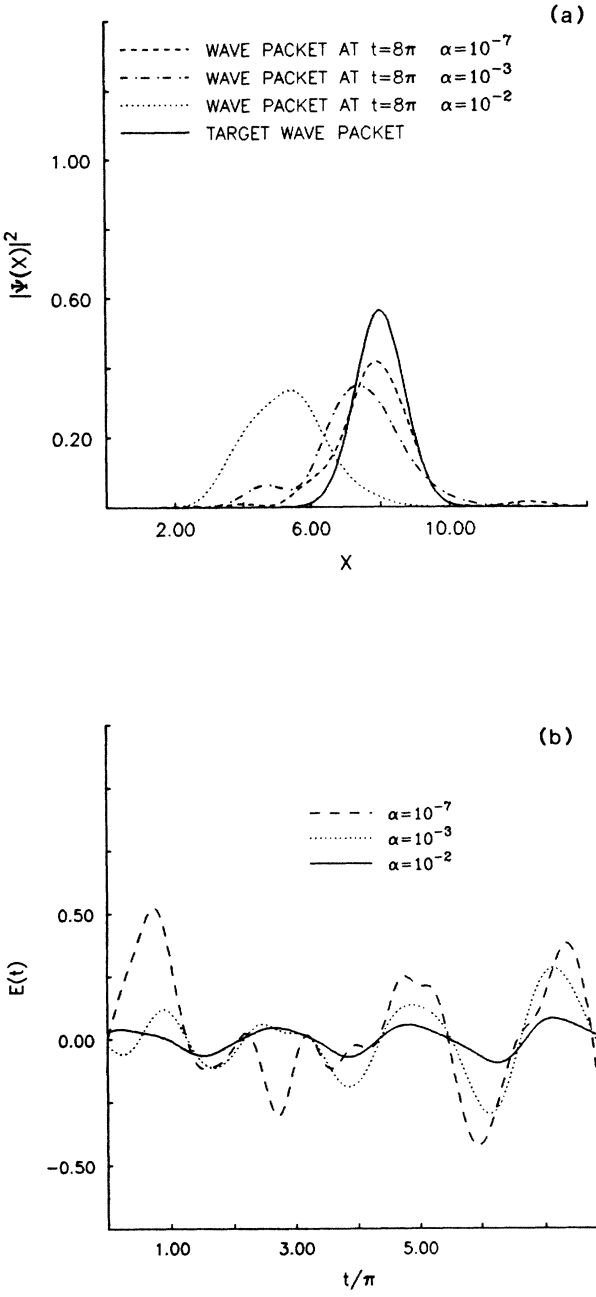

FIG. 3. Three distinct wave packets, each corresponding to different values of α. The parameter α determines the relative importance between the term that represents error in achieving the target state $\hat{\psi}$, and the magnitude of the applied potential. In each case a spatially constrained applied potential of the form $-(X-4)E(t)$ is sought. (a) The probability densities at time $T=8\pi$ of the three wave packets and that of the target. Initially $\psi_0(X)=g(X,4,1)$ and the final target at time T is $\hat{\psi}(X)=g(X,8,1)$ for each of the wave packets. (b) The applied electric field $E(t)$ for each of the values of α. As α is increased the magnitude of the applied field is restricted, which limits the extent to which the target state $\hat{\psi}$ can be achieved as can be seen in (a). As a result of an increase in α the applied field $E(t)$ also loses some of the important phase adjustment structure as can be seen clearly in the early time interval $[0,4\pi]$ upon comparison of the cases $\alpha=10^{-3}$ and 10^{-7} in (b). All the quantities used in this figure are dimensionless.

molecular control problems other terms may enter into the cost functional with a correspondingly greater choice to be made as to their relative weight. This prospect provides an important degree of flexibility and in favorable cases a family of satisfactory field designs might be obtained.

D. A model of dissociation

A question of practical importance is to determine the appropriate externally applied potential that will drive the wave packet out of the potential well. Although radiative dissociation of diatoms has been demonstrated in an uncontrolled framework, we consider radiative dissociation here using optimal control theory with a view to its real utility in polyatomic applications. There is a variety of ways in which this can be formulated in terms of the optimal control problem (2.1). If, for example, we consider Gaussian target wave packets of the form

$$\hat{\psi}(x)=g(X,X_f,l_f)\exp[-iP_fX/\hbar]\ , \tag{5.6}$$

where g is defined in (5.4), then the target energy $\hat{\mathcal{E}}:=\langle\hat{\psi},H_0\hat{\psi}\rangle_X$ can be made larger than the dissociation energy of 5.0 in the present case by choosing X_f, P_f, and l_f appropriately. If we determine a control $B(X)E(t)$,

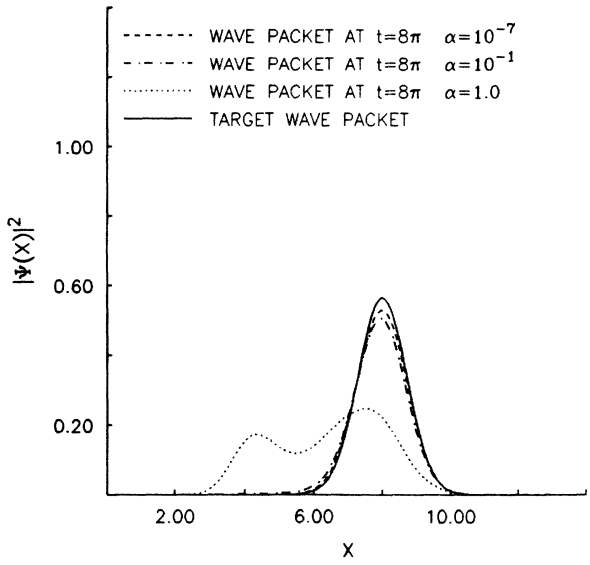

FIG. 4. Probability density at time $T=8\pi$ of three distinct wave packets, each corresponding to different values of α. The parameter α determines the relative importance in the cost functional $J[u]$ of the term representing the error in achieving $\hat{\psi}$ with the term representing the magnitude of the applied field $u(X,t)$. Initially the wave packets are all Gaussian, i.e., $\psi_0(X)=g(X,X_0=4,1)$ and targeted to be the same Gaussian centered at $X_f=8.0$ at time T, i.e., $\hat{\psi}(X)=g(X,8,1)$. In each case an unconstrained applied potential of the form $u(X,t)$ is sought. As the magnitude of u is forced to be smaller by increasing α, the reachability of the target state $\hat{\psi}$ can be seen to diminish. All the quantities used in this figure are dimensionless.

which ensures that $\|\psi-\hat{\psi}\|_X$ is sufficiently small, then implicitly we will have established a control that achieves dissociation at the given time T. It might be argued that this control will not necessarily be the one that requires the least energy or some other criterion to achieve dissociation. However, accepting the fact that the optimization takes place over a subset of dissociation controllers determined by the problem posed in (2.1), the solution to the model problem we have posed does yield an optimal controller that will achieve dissociation in a given time T.

In this section we shall use a spatially constrained con-

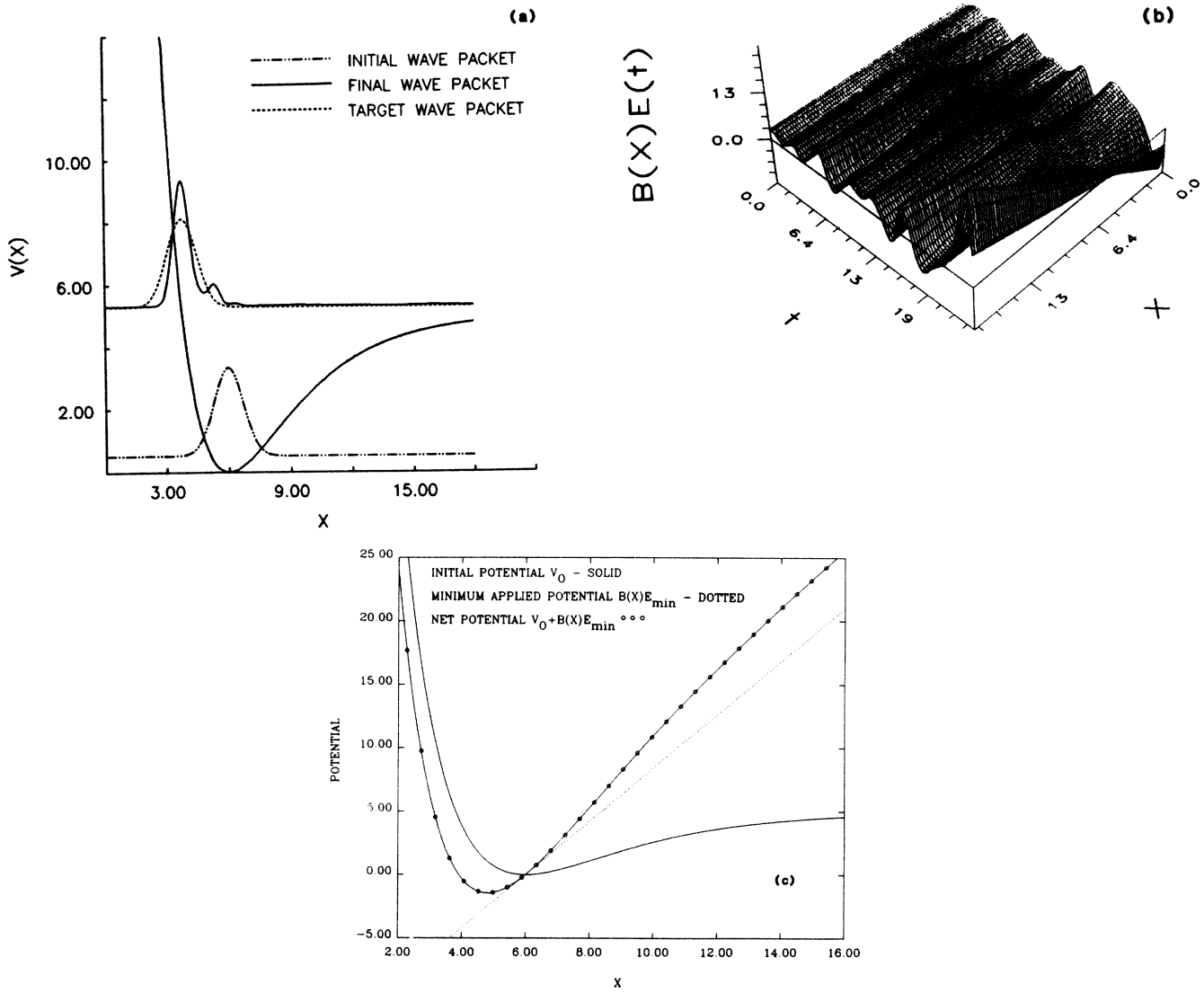

FIG. 5. A model of dissociation obtained by requesting that a Gaussian wave packet be translated from $X_0=6.0$ to $X_f=3.8$ in the given time $T=8\pi$. A spatially constrained potential of the form (P1):$-(X-6)E(t)$ is sought to achieve dissociation by bond compression and release at time T. (a) The initial potential $V_0(X)$ on which the probability densities of $\psi_0(X)$, $\psi(X,T)$, and $\hat{\psi}(X)$ have been superimposed at their appropriate energy levels. The final wave packet has sufficient energy for dissociation of the molecule to take place. (b) The external applied potential over the space-time domain $[0,18]\times[0,8\pi]$. At any instant of time the spatial form of this external potential is a linear ramp of positive or negative slope. This alternating ramp when combined with the Morse potential $V_0(X)$ provides the control for guiding the wave packet to the desired final objective. (c) The Morse potential $V_0(X)$, the applied potential corresponding to the minimum value $E_{\min}$. The enhanced curvature of the net potential in the target region $X=3.8$ provides an explanation for the narrowing of the final wave packet that can be seen in (a). A figure analogous to 1(c) also applies in this case for $E_{\max}$. (d) The plot of the electric field $E(t)$ over the time interval $[0,8\pi]$ is positioned above the contour plot of the probability density $|\psi(X,t)|^2$ over the space-time domain $[0,18]\times[0,8\pi]$. The response of the wave packet to the driving electric field $E(t)$ can be observed. The field tends to lead the wave packet by a time period of approximately $\pi/2$. Initially there is a time period of phase adjustment, which is relatively high in frequency and low in amplitude. This is followed by a large low-frequency pulse which is applied near the end of the time interval $[0,8\pi]$. This last pulse provides the guidance to squeeze the molecular bond to its desired target. (e) The energy $\mathcal{E}(t)$ of the wave packet over the time interval $[0,8\pi]$. The electric field $E(t)$ is superimposed on this plot (see the dashed curve). The large pulse in $E(t)$ that occurs toward the end of the time interval $[0,8\pi]$, can be seen to cause the major energy transfer to the wave packet. All the quantities used in this figure are dimensionless.

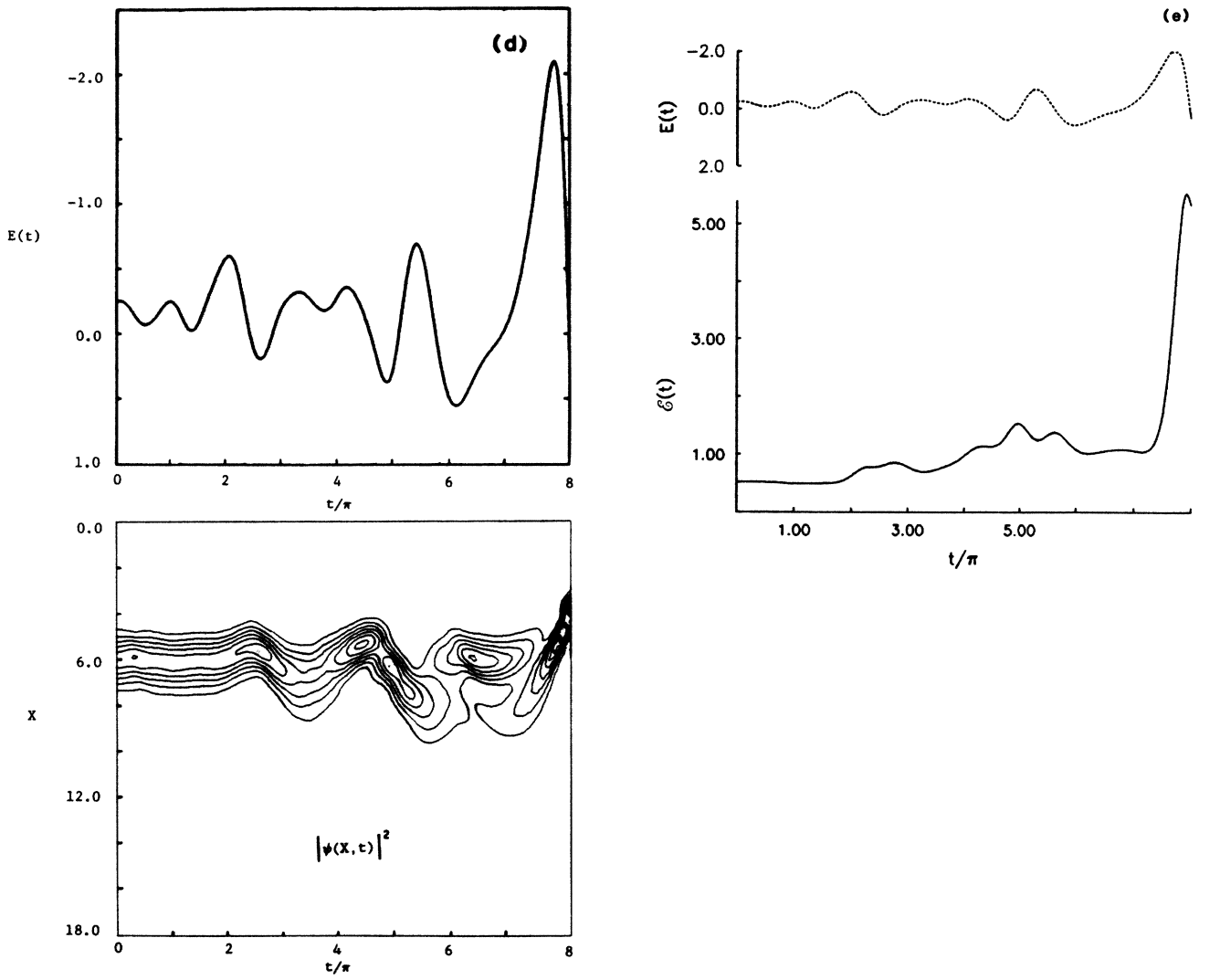

FIG. 5. (*Continued*).

troller of the form $B(X)E(t)=-(X-X_0)E(t)$. We choose $L=18.0$ and the bottom of the potential well at $X_0=6.0$. In this case, dissociation is sought by varying the field to sufficiently compress the molecule at time T and then release it to fly apart. In order for the target wave packet $\hat{\psi}(x)$ defined in (5.7) to have sufficient energy to ensure that $\hat{\mathcal{E}}>5$, we choose $X_f=3.8$, $P_f=0.0$, and $l_f=1.0$. We assume a Gaussian initial wave packet of width 1.0 and centered at $X_0=6.0$ so that

$$\psi_0(X)=g(X,6,1)\ .$$

In Fig. 5(a) the initial, final, and target probability distributions of the wave packet are superimposed on the potential V_0 at the appropriate energy levels. As the figure demonstrates, the final wave packet has sufficient energy for dissociation to take place. The probability distribution $|\psi(X,T)|^2$ of the final wave packet is narrower than that of the target $|\hat{\psi}(X)|^2$. This can be explained by the fact that the external applied potential $-(X-X_0)E(t)$ pivots about X_0 [see Fig. 5(b)] and that the gradient of the potential $V_0(X)$ increases as X decreases away from X_0. As a result, a significant effective curvature of the combined potential $V_0(X)-(X-X_0)E(t)$ can be achieved in the region $X<X_0$ by decreasing $E(t)$ sufficiently. This increased curvature is demonstrated in Fig. 5(c) in which the initial potential $V_0(X)$, the applied potential for the minimum field $E_{\min}$, and the net potential $V_0(X)-(X-X_0)E_{\min}$ are plotted. We observe that in the target region $X_f=3.8$, the curvature of the net potential is increased significantly relative to that of V_0. This causes the narrowing of the final wave packet seen in Fig. 5(a). Contrasting the sharpening effect observed here with the broadening effect observed in Sec. V B for the same class of constrained controllers, we see that the joint interaction of the molecular Hamiltonian H_0 with the form of the dipole function $B(X)$ makes certain target wave packets reachable in some regions but unattainable in others.

In Fig. 5(d) the plot of $E(t)$ is positioned above the space-time contour plot of the corresponding probability density $|\psi(x,t)|^2$. The function $E(t)$ is proportional to that which forms the boundary of the surface $B(X)E(t)$ at $X=18.0$, which is plotted in Fig. 5(b). As was the case in Fig. 1, the wave packet lags behind the larger peaks of

$E(t)$. Very little excitation is performed by the controller for $t \in [0, 2\pi]$. In fact, during the interval $[0, 5\pi]$, the strategy of the controller is to produce low-amplitude phase adjustments. This is followed by a large low-frequency pulse toward the end of the interval $[0, T]$. The large peak of $E(t)$ near the end of the interval increases the effective curvature of the combined potential as was demonstrated in Fig. 5(c). This results in the narrowing of the wave packet near the end of the interval $[0, 8\pi]$, which can be seen clearly in the contour plot and manifests itself in the width of the final wave packet. In Fig. 5(e) the time evolution of the energy $\mathcal{E}(t)$ of the wave packet is plotted. Superimposed on this plot is the applied field $E(t)$, which is represented by a dotted line. The phase adjustment stage does little to the energy of the wave packet. The majority of the energy transfer to the wave packet can be seen to result from the large low-frequency pulse applied at the end of the interval. The *average* energy involved in applying the external potential, as measured by the functional defined in (5.5), is in this case $\mathcal{E}[BE] = 0.38$.

We have thus demonstrated that it is possible to determine, using this model dissociation problem, a pulsing strategy that achieves dissociation in the given time interval and that is optimal in the sense of the optimal control problem posed in (2.1). The optimal field $E(t)$ exhibits a number of interesting features that could not have been anticipated *a priori* without such an analysis. In this case as well as that of Fig. 1 control and guidance of the wave packet is achieved by batting the wave packet back and forth in a delicately phased fashion by means of the applied potential $B(X)E(t)$.

VI. COMMENTS AND CONCLUSIONS

We have formulated an optimal control problem for the time-dependent Schrödinger equation. The issue of the well-posedness of the optimal control problem was considered and the existence of a solution to the problem was demonstrated. Using the technique of Lagrange multipliers we derived necessary conditions for a minimum of the optimization problem. These necessary conditions form the basis of a gradient-based algorithm to search for a minimum. A numerical strategy was proposed requiring implicit integration using the Crank-Nicholson scheme because the applied potential was not known *a priori*. A number of numerical experiments were performed with the following objectives.

(i) To verify that the numerical solution to the optimization problem does indeed yield a solution that results in a specific target state being achieved within a given time T.

(ii) To demonstrate the effect of the parameter α that balances the two terms in the cost functional J.

(iii) To provide a numerical solution to a model of dissociation in which an appropriate pulsing strategy is sought that will ensure dissociation in a given time.

In each of the problems considered the applied potential exhibited an interesting detailed structure that could not be anticipated *a priori*. This illustrates the usefulness of a control-theory approach to achieving quantum-dynamical objectives. An issue not explored here was the sensitivity of the final solution to the value of the time T taken for the solution to be reached. In another work[13] it was shown that the field $E(t)$ near the end point T takes on a specific limiting form as T grows. Optimal control theory thus provides a promising approach to the search for an appropriate pulsing strategy. If it is to become a practical design tool, a number of issues need to be addressed including the following.

(i) Computational efficiency: The solution of the time-dependent Schrödinger equation for practical problems is in itself a computationally expensive venture. The optimization problem is even more computationally intensive, involving the solution of a large number of time-dependent Schrödinger problems before a minimum can be achieved. For example, each of the numerical experiments performed typically involved approximately 30 CPU hours on a Micro-Vax II computer.

It can therefore be seen that the development of more efficient schemes for the numerical solution of the Schrödinger equation and the optimization problem itself may prove to be essential if practical polyatomic problems are to be tractable. For progress in this area the reader is referred to the work of Kosloff.[29]

(ii) Reformulation: If a practical dissociation problem were considered, then a reformulation in which the observables (e.g., the energy) appear in the cost functional would be more appropriate.

(iii) Robustness: The design of a robust controller that is insensitive to uncertainties in the Hamiltonian, the molecular dipole function, and initial conditions will be essential for practical problems.[30] In addition, insensitivity to laboratory field errors would also be very important. The imposition of practical levels of insensitivity is essential since implementation of the field designs in the laboratory will, of necessity, be of an open-loop[9] nature.

We have formulated an optimal control problem that is shown to be well-posed, tractable and which yields useful information about pulsing strategies for quantum systems. Although this is an exploratory investigation of an idealized system, it highlights essential features of what could become a useful design tool.

ACKNOWLEDGMENTS

The authors acknowledge support for this research from the U.S. Office of Naval Research and the U.S. Air Force Office of Scientific Research. The first author also gratefully acknowledges the support of the Council of Scientific and Industrial Research of South Africa and the Fulbright Foundation.

[1]A. Garroway, P. Grannell, and P. Mansfield, J. Phys. C **7**, L457 (1974).
[2]R. Sutherland and J. Hutchinson, J. Phys. E **11**, 79 (1978).
[3]D. Hoult, J. Magn. Reson. **35**, 69 (1979).
[4]N. Bloembergen and A. H. Zewail, J. Phys. Chem. **88**, 5459 (1984).
[5]P. Lochner, Philos. Trans. R. Soc. London, Ser. B **289**, 537 (1980).
[6]W. Loeffler, A. Oppelt, and D. Faul (unpublished).
[7]R. B. Walker and R. K. Preston, J. Chem. Phys. **67**, 2017 (1977).
[8]P. S. Dardi and S. K. Gray, J. Chem. Phys. **77**, 1345 (1982).
[9]A. E. Bryson and Y. Ho, *Applied Optimal Control* (Hemisphere, Washington, D.C., 1975).
[10]D. G. Luenberger, *Introduction to Dynamic Systems* (Wiley, New York, 1979).
[11]S. Conolly and A. Macovski (unpublished).
[12]S. Conolly, D. Nishimura, and A. Macovski, IEEE Med. Im. **5**, 106 (1986).
[13]A. Woody, S. Shi, and H. Rabitz, J. Chem. Phys. (to be published).
[14]S. Shi and H. Rabitz (unpublished).
[15]D. J. Tannor and S. A. Rice, J. Chem. Phys. **83**, 5013 (1985).
[16]D. J. Tannor, R. Kosloff, and S. A. Rice, J. Chem. Phys. **85**, 5805 (1986).
[17]S. A. Rice and D. J. Tannor, J. Chem. Soc. Faraday Trans. 2 **82**, 2423 (1986).
[18]A. G. Butkovskii and Y. I. Samoilenko, Autom. Remote Control (USSR) **A**, 485 (1979).
[19]A. G. Butkovskii and Y. I. Samoilenko, Dokl. Akad. Nauk SSSR, **250**, 51 (1980).
[20]G. M. Huang, T. J. Tarn, and J. W. Clark, J. Math. Phys. **24**, 2608 (1983).
[21]V. P. Belavkin, in Proceedings of the 7th All Union Conference on Encoding and Transmission of Information, Vilnius 1978 (in Russian) [Nauchn. Sovet Kompleks. Probl. Kibern. Akad. Nauk SSSR **1**, 23 (1978)].
[22]E. V. Davies, IEEE Trans. Inf. Theory, **IT-23**, 530 (1977).
[23]A. V. Balakrishnan, *Applied Functional Analysis,* 2nd ed. (Springer-Verlag, New York, 1981).
[24]A. Pazy, *Semigroups of Linear Operators and Applications to Partial Differential Equations* (Springer-Verlag, New York, 1983).
[25]D. G. Luenberger, *Optimization of Vector Space Methods* (Wiley, New York, 1969).
[26]D. G. Luenberger, *Linear and Nonlinear Programming,* 2nd ed. (Addison-Wesley, Reading, MA, 1984).
[27]G. D. Smith, *Numerical Solution of Partial Differential Equations: Finite Difference Methods,* 2nd ed. (Oxford University Press, Oxford, 1978).
[28]A. Askar and A. S. Cakmak, J. Chem. Phys. **68**, 2794 (1978).
[29]D. Kosloff and R. Kosloff, J. Comput. Phys. **52**, 35 (1983).
[30]M. A. Dahleh, Ph.D. dissertation, Princeton University, 1987.

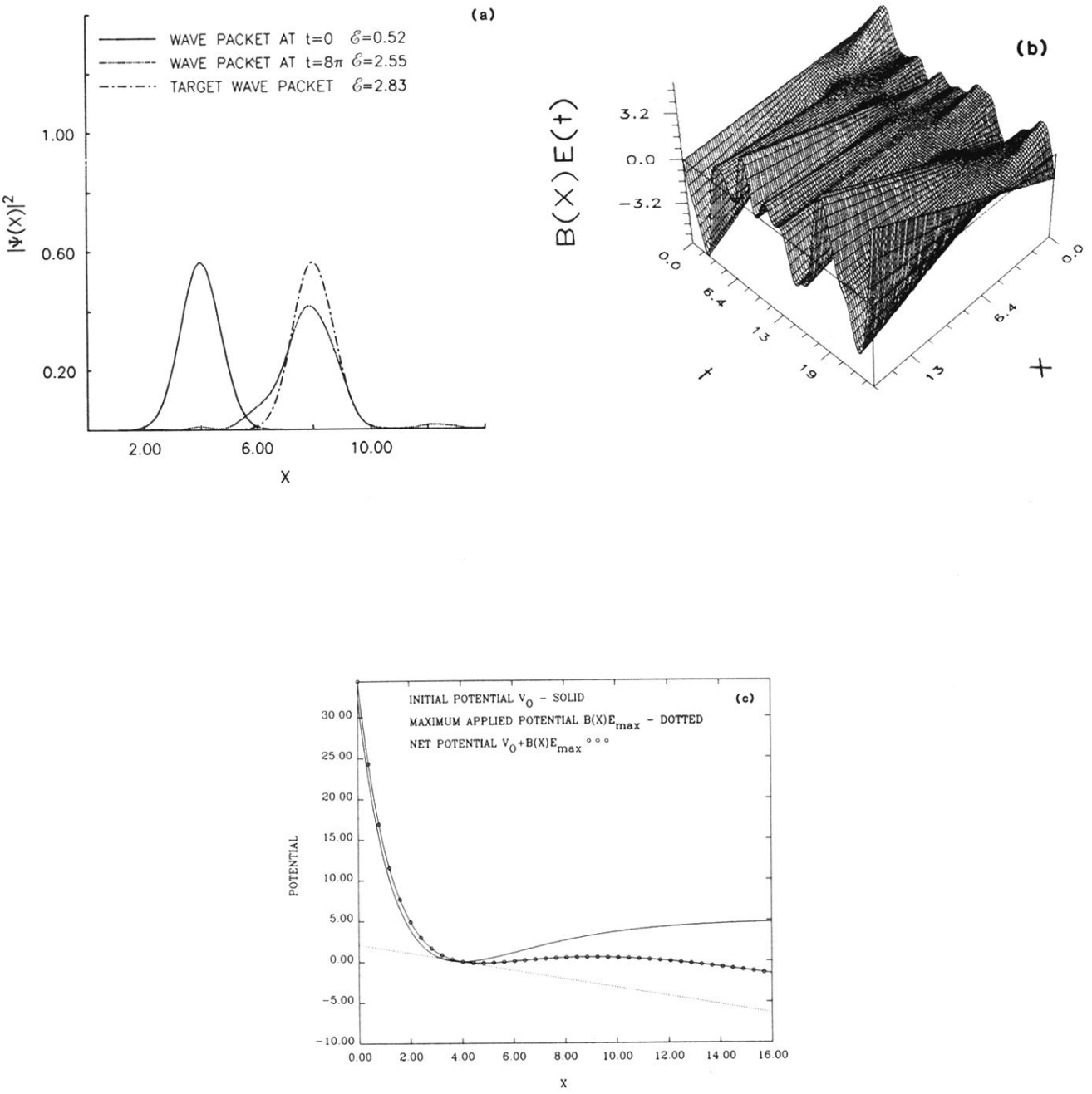

FIG. 1. A Gaussian wave packet translated from $X_0=4.0$ to $X_f=8.0$ by a spatially constrained external applied potential (P1) $B(X)E(t)=-(X-X_0)E(t)$. (a) The probability densities of the initial wave packet $\psi_0(X)$, the final wave packet $\psi(X,T)$ achieved using $B(X)E(t)$, and the target wave packet $\hat{\psi}(X)$. (b) The external applied potential $B(X)E(t)$ over the space-time domain $[0,16.0]\times[0,8\pi]$. At any instant of time the spatial form of this external potential is a linear ramp of positive or negative slope. This alternating ramp, when combined with the Morse potential $V_0(X)$, provides the control for guiding the wave packet to the desired final objective. (c) The Morse potential $V_0(X)$, the applied potential corresponding to the maximum value $E_{\max}$ of $E(t)$, and the net potential $V_0(X)+B(X)E_{\max}$. The negative curvature of the net potential in the target region $X=8.0$ explains the spreading of the final wave packet shown in (a). (d) The plot of the electric field $E(t)$ over the time interval $[0,8\pi]$ is positioned above the contour plot of the probability density $|\psi(X,t)|^2$ over the space-time domain $[0,16]\times[0,8\pi]$ so that the time intervals are aligned. The response of the wave packet to the driving electric field can be observed. The field tends to lead the wave packet by a time period of approximately $\pi/2$. There are two pulses at $t=\pi$ and 6π which are low frequency and have relatively large amplitudes. Between these two pulses there is a stage of higher-frequency phase adjustment. (e) The power spectrum of $E(t)$, i.e., the magnitude of the discrete Fourier transform normalized to unity. The rightmost peak corresponds to the fundamental frequency $\omega=1.0$. The occurrence of some higher-frequency components with lower amplitudes is consistent with the phase adjustment stage. (f) The energy $\mathcal{E}(t)$ of the wave packet over the time interval $[0,8\pi]$. The electric field $E(t)$ is superimposed on this plot (see dashed curve). The correspondence between the larger-amplitude pulses in $E(t)$ and the deposition of energy to the molecular wave packet can be observed. All the quantities used in this figure are dimensionless.

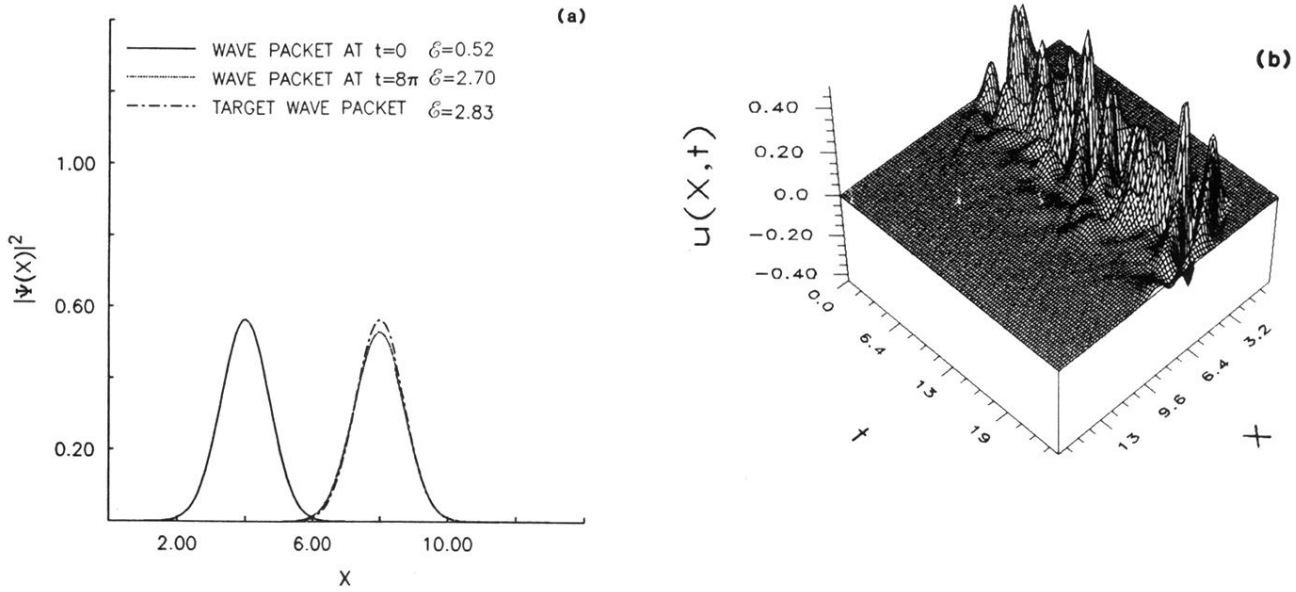

FIG. 2. A Gaussian wave packet translated from $X_0=4.0$ to $X_f=8.0$ by an unconstrained applied potential (P2) $u(X,t)$. (a) The probability densities of the initial wave packet $\psi_0(X)$, the final wave packet $\psi(X,T)$ achieved using $u(X,t)$, and the target wave packet $\hat{\psi}(X)$. (b) The external applied potential $u(X,t)$ over the space-time domain $[0,16.0]\times[0,8\pi]$. The spatially localized, complex structure of this potential should be contrasted with that of the constrained potential shown in Fig. 1(b). (c) Three space-time plots with an aligned time interval. (i) Regions of positive (dark shading) and negative (light shading) applied potential $u(X,t)$. (ii) A contour plot of the probability density $|\psi(X,t)|^2$ with contour intervals $\Delta|\psi|^2=0.1$. (iii) Positive and/or negative regions of the flux vector $\mathbf{J}(X,t)$. The positive regions (dark shading) represent regions in which there is a flux of material in the positive-X direction, whereas negative regions (light shading) represent regions in which the flux of material is in the negative-X direction. A similar period to that of Fig. 1 of high-frequency phase adjustment can be observed. This is followed by a stage in which the wave packet is guided to the objective by a deepening well indicated by the dashed line. The same dashed line on the contour plot of the probability density demonstrates the phase lag of the wave packet behind the external excitation. The large uninterrupted regions of material flux confirm that the wave packet is being chanelled to the final state toward the end of the interval $[0,8\pi]$. (d) The energy $\mathcal{E}(t)$ of the wave packet over the time interval $[0,8\pi]$. In this case the energy absorption of the wave packet is monotonic, which was not the case for the spatially constrained controller [see Fig. 1(f)]. All the quantities used in this figure are dimensionless.

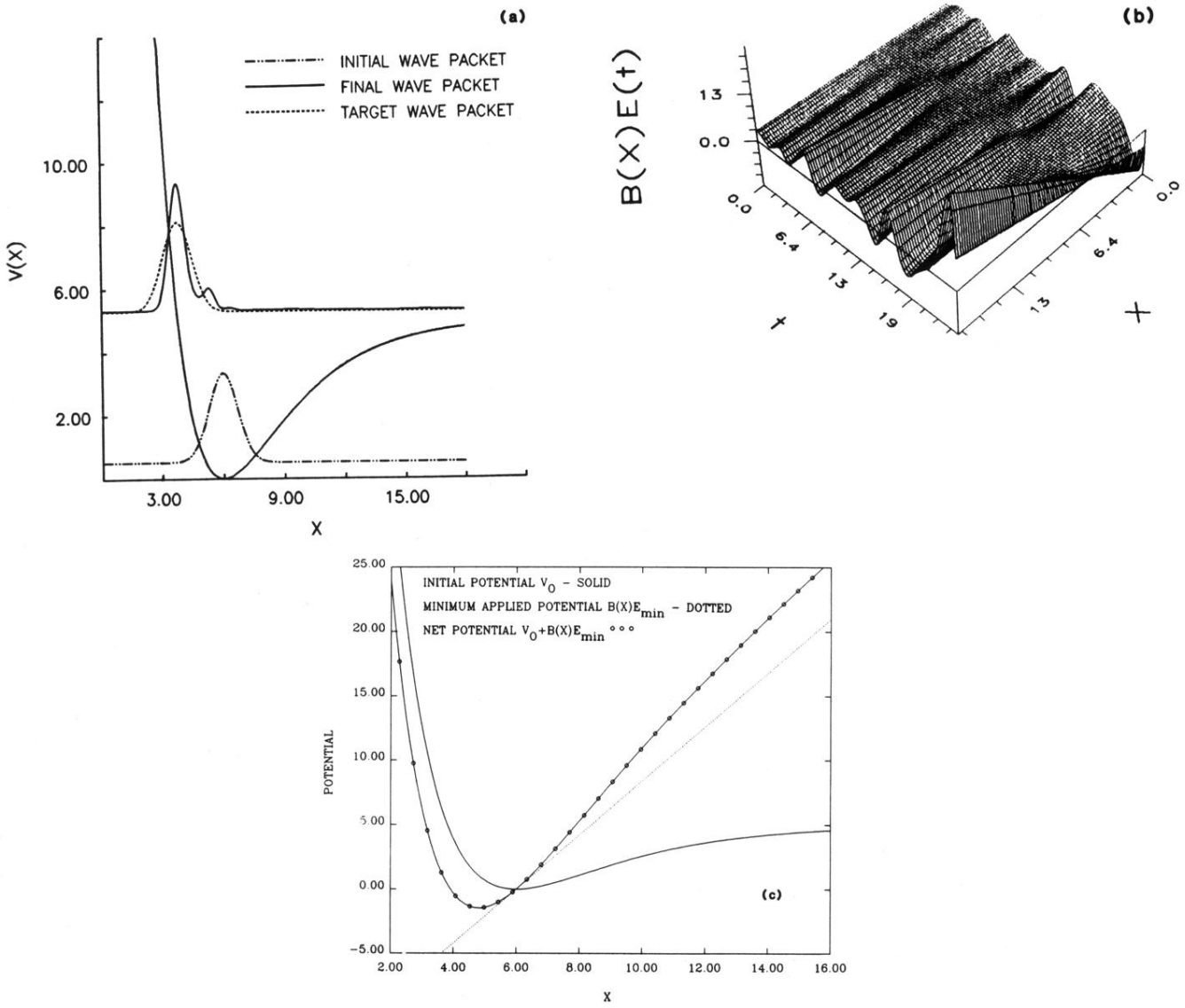

FIG. 5. A model of dissociation obtained by requesting that a Gaussian wave packet be translated from $X_0=6.0$ to $X_f=3.8$ in the given time $T=8\pi$. A spatially constrained potential of the form (P1):$-(X-6)E(t)$ is sought to achieve dissociation by bond compression and release at time T. (a) The initial potential $V_0(X)$ on which the probability densities of $\psi_0(X)$, $\psi(X,T)$, and $\hat{\psi}(X)$ have been superimposed at their appropriate energy levels. The final wave packet has sufficient energy for dissociation of the molecule to take place. (b) The external applied potential over the space-time domain $[0,18]\times[0,8\pi]$. At any instant of time the spatial form of this external potential is a linear ramp of positive or negative slope. This alternating ramp when combined with the Morse potential $V_0(X)$ provides the control for guiding the wave packet to the desired final objective. (c) The Morse potential $V_0(X)$, the applied potential corresponding to the minimum value $E_{\min}$. The enhanced curvature of the net potential in the target region $X=3.8$ provides an explanation for the narrowing of the final wave packet that can be seen in (a). A figure analogous to 1(c) also applies in this case for $E_{\max}$. (d) The plot of the electric field $E(t)$ over the time interval $[0,8\pi]$ is positioned above the contour plot of the probability density $|\psi(X,t)|^2$ over the space-time domain $[0,18]\times[0,8\pi]$. The response of the wave packet to the driving electric field $E(t)$ can be observed. The field tends to lead the wave packet by a time period of approximately $\pi/2$. Initially there is a time period of phase adjustment, which is relatively high in frequency and low in amplitude. This is followed by a large low-frequency pulse which is applied near the end of the time interval $[0,8\pi]$. This last pulse provides the guidance to squeeze the molecular bond to its desired target. (e) The energy $\mathcal{E}(t)$ of the wave packet over the time interval $[0,8\pi]$. The electric field $E(t)$ is superimposed on this plot (see the dashed curve). The large pulse in $E(t)$ that occurs toward the end of the time interval $[0,8\pi]$, can be seen to cause the major energy transfer to the wave packet. All the quantities used in this figure are dimensionless.